

Article

# Room Temperature Solid State Synthesis, Characterization, and Application of a Zinc Complex with Pyromellitic Acid

Rong-Gui Yang, Mei-Ling Wang, Ting Liu and Guo-Qing Zhong \* 

School of Material Science and Engineering, Southwest University of Science and Technology, Mianyang 621010, China; yangronggui@mails.swust.edu.cn (R.-G.Y.); wangmeiling160206@163.com (M.-L.W.); liuting0906@mails.swust.edu.cn (T.L.)

\* Correspondence: zgq316@163.com or zhongguoqing@swust.edu.cn; Tel.: +86-816-6089371

Received: 31 December 2017; Accepted: 22 January 2018; Published: 24 January 2018

**Abstract:** The complex  $[\text{Zn}_2(\text{btca})(\text{H}_2\text{O})_4]$  was synthesized with 1,2,4,5-benzenetetracarboxylic acid ( $\text{H}_4\text{btca}$ ) and zinc acetate as materials via a room-temperature solid state reaction. The composition and structure of the complex were characterized by elemental analyses (EA), Fourier transform infrared spectroscopy (FTIR), X-ray powder diffraction (XRD), and thermogravimetric (TG) analysis. The index results of X-ray powder diffraction data showed that the crystal structure of the complex belonged to monoclinic system with cell parameters  $a = 9.882 \text{ \AA}$ ,  $b = 21.311 \text{ \AA}$ ,  $c = 15.746 \text{ \AA}$ , and  $\beta = 100.69^\circ$ . In order to expand the application of the complex, the nanometer zinc oxide was prepared by using the complex as a precursor, and the effect of the thermal decomposition temperature on the preparation of the nanometer zinc oxide was studied. The results showed that the grain size of zinc oxide gradually grew with the increase of the pyrolysis temperature, the obtained nanometer zinc oxide was spherical, and the diameter of the particles was about 25 nm.

**Keywords:** room-temperature solid state reaction; zinc complex; index of X-ray powder diffraction data; precursor; nanometer zinc oxide

## 1. Introduction

Pyromellitic acid, namely 1,2,4,5-benzenetetracarboxylic acid ( $\text{H}_4\text{btca}$ ), is usually used as a ligand for the synthesis of the complexes. There are four carboxyl groups in the pyromellitic acid, which leads to a rich variety of coordination patterns and topological structures [1–3]. The tetra-anion of  $\text{H}_4\text{btca}$  is interesting as a suitable ligand for the preparation of inorganic–organic framework structures. At the same time, the existence of aromatic ring in pyromellitic acid is conducive to the transfer of the electrons, which contributes to the preparation of optical, electrical and magnetic chemical materials [4–7]. The common synthetic method for this kind of complexes is the solvothermal method, and the complexes synthesized by this method have protean structures and superior performances [8,9]. However, there are some shortcomings for the method, such as difficult controls of synthetic conditions and difficulty in understanding the reaction process.

The nanophase materials have the distinctive surface effect, volume effect, macroscopic quantum tunneling effect, and so on. As a result, nanomaterials can be applied to the fields of electricity, magnetism, optics, mechanics, catalysis, energy, explosives, and as a combustion improver. The studies and preparation of nano-ZnO have attracted more and more attention globally; for example, the development of nanometer zinc oxide is included in the “863 Plan” in China. There are many methods used to prepare nano-ZnO in laboratory [10–14], which can be divided into chemical methods and physical methods. Among them, chemical methods are more studied, especially the thermal decomposition of zinc complexes with organic acid.

In this paper, the zinc complex of pyromellitic acid was synthesized via a room temperature solid state reaction, and the complex was used as precursor to prepare the nano-ZnO. This synthetic method of this complex is not only easy to operate, but it has a high yield.

## 2. Experimental Section

### 2.1. Materials and Physical Measurements

All chemicals purchased were of analytical reagent grade and used without further purification. Zinc acetate ( $\text{Zn}(\text{Ac})_2 \cdot 2\text{H}_2\text{O}$ ) was purchased from Sinopharm Chemical Reagent Co., Ltd. (Shanghai, China) and 1,2,4,5-benzenetetracarboxylic acid ( $\text{H}_4\text{btca}$ ) was obtained from Jinan Henghua Sci. and Tec. Co., Ltd. (Jinan, China).

Elemental analyses for C, H, and O in the complex were measured on a Vario EL CUBE elemental analyzer (Elementar, Langensfeld, Germany), and the content of zinc was determined by EDTA complexometric titration with chrome black T as indicator. FTIR spectra were obtained with KBr pellets on a Nicolet 5700 FT-IR spectrophotometer (ARCOptix, Neuchatel, Switzerland) in the range of  $4000\text{--}400\text{ cm}^{-1}$ . The powder X-ray diffraction data were collected on a D/max-II X-ray diffractometer (Rigaku, Tokyo, Japan) with  $\text{Cu K}\alpha_1$  radiation, the voltage of 35 kV, the current of 60 mA, and the scanning speed of  $8^\circ\text{ min}^{-1}$ , in the diffraction angle range of  $3\text{--}80^\circ$ . The thermogravimetric analysis data were obtained using a SDT Q600 thermogravimetry analyzer (TA Instruments, New Castle, DE, USA) in an air atmosphere in the temperature range of  $25\text{--}800^\circ\text{C}$  with a heating rate of  $10^\circ\text{C min}^{-1}$ . Scanning electron microscope (SEM) images of particles were measured on an Ultra 55 field emission scanning electron microscope system (Camcor, Inc., Burlington, NC, USA).

### 2.2. Synthesis of $[\text{Zn}_2(\text{btca})(\text{H}_2\text{O})_4]$

$\text{Zn}(\text{Ac})_2 \cdot 2\text{H}_2\text{O}$  (4.39 g, 20 mmol) and  $\text{H}_4\text{btca}$  (2.54 g, 10 mmol) were weighed and the mixture was placed in a mortar. There was a pungent-smelling gas due to acetic acid generation when grinding the mixture. The mixture was ground for about 30 min at room temperature and then placed in a constant-temperature drying oven with  $60^\circ\text{C}$ . After 10 min, the mixture was continued to be ground. These steps were repeated until there was no pungent-smelling gas produced. The product was a white powder (4.18 g) and the yield was about 92.3%.

### 2.3. Preparation of Nano-ZnO

The complex  $[\text{Zn}_2(\text{btca})(\text{H}_2\text{O})_4]$  was respectively calcined at  $400^\circ\text{C}$ ,  $500^\circ\text{C}$ , and  $600^\circ\text{C}$  for 1.5 h, and the nano-ZnO with a narrow size distribution was obtained. The effect of the calcination temperature on the particle size of nano-ZnO was explored.

## 3. Results and Discussion

### 3.1. Composition and Property of the Title Complex

Anal. Calc. (%) for the title complex  $\text{C}_{10}\text{H}_{10}\text{O}_{12}\text{Zn}_2$ : C, 26.51; H, 2.23; O, 42.39; Zn, 28.87. Found (%): C, 26.37; H, 2.27; O, 42.62, Zn, 28.74. The experimental results coincide with the theoretical calculation. The complex consists of two zinc cations, one  $\text{btca}^{4-}$  anion, and four water molecules. According to the results of FTIR and thermal analysis, the composition of the complex is  $[\text{Zn}_2(\text{btca})(\text{H}_2\text{O})_4]$  ( $M_r = 452.96$ ). Every Zn(II) ion is coordinated by four oxygen atoms from two carboxyl groups on the same side of the  $\text{btca}^{4-}$  ligand and two coordinated water molecules, which forms a distorted tetrahedral configuration, and the molecular structure of the complex is shown in Figure 1. The complex is fairly stable at room temperature and has no moisture absorption.

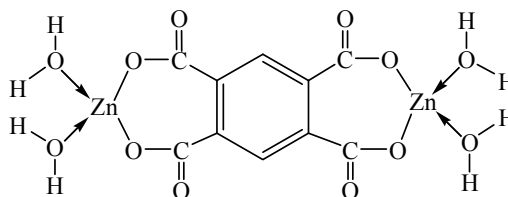


Figure 1. Molecular structure of  $[Zn_2(btca)(H_2O)_4]$ .

### 3.2. X-ray Powder Diffraction Analysis

The XRD pattern of the complex is shown in Figure 2. The baseline of the XRD pattern is low and the intensity of the diffraction peak is strong, which indicates that the complex has a good crystalline state. The three main strong peaks appear in  $2\theta = 15.44^\circ$ ,  $18.98^\circ$ , and  $21.88^\circ$  for the complex, and in  $2\theta = 25.80^\circ$ ,  $28.97^\circ$ , and  $11.76^\circ$  for pyromellitic acid (JCPDS No. 13-0882), while in  $2\theta = 11.26^\circ$ ,  $19.62^\circ$ , and  $22.55^\circ$  for zinc acetate (JCPDS No. 21-1467). Comparing with the reactants, the strong peak locations in XRD pattern of the complex are obviously changed. In short, all of these strong peaks in the XRD patterns of the reactants are disappeared in the XRD pattern of the complex. The diffraction angle ( $2\theta$ ), diffractive intensity, and spacing ( $d$ ) of the resultant are completely different from the reactive materials, which may illuminate that the resultant is a new compound instead of the reactant mixture [15].

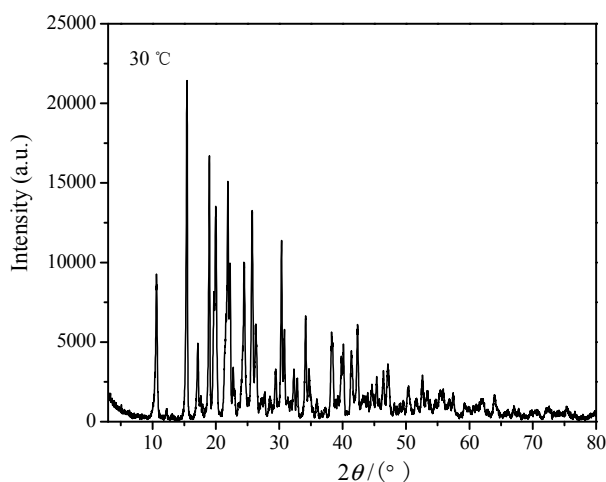


Figure 2. XRD pattern of  $[Zn_2(btca)(H_2O)_4]$ .

The index calculation of the XRD data bases on the computer program of least squares method [16], and the calculated results are shown in Table 1. All of the XRD data of the complex can be calculated according to the monoclinic system. The calculated interplanar spacing is consistent with the measured value, and the largest relative deviation between the experimental and calculated spacing  $d_{hkl}$  is less than 0.3%. As a result, the resultant is a single phase compound, and the crystal structure of the complex belongs to monoclinic system, and its cell parameters are  $a = 9.882 \text{ \AA}$ ,  $b = 21.311 \text{ \AA}$ ,  $c = 15.746 \text{ \AA}$ , and  $\beta = 100.69^\circ$ .

Table 1. Experimental data and calculated results for XRD of  $[Zn_2(btca)(H_2O)_4]$ .

No.	$2\theta/^\circ$	$h$	$k$	$l$	$d_{\text{exp}}/\text{\AA}$	$d_{\text{cal}}/\text{\AA}$	$I/I_0$	No.	$2\theta/^\circ$	$h$	$k$	$l$	$d_{\text{exp}}/\text{\AA}$	$d_{\text{cal}}/\text{\AA}$	$I/I_0$
1	10.64	1	1	-1	8.308	8.300	42.4	29	39.80	1	7	4	2.263	2.263	15.6
2	15.44	1	3	0	5.734	5.733	100.0	30	40.14	2	4	-6	2.245	2.245	20.2
3	17.14	0	0	3	5.169	5.158	21.9	31	41.40	1	7	-5	2.179	2.179	18.2
4	17.61	0	4	1	5.034	5.037	5.9	32	42.36	2	9	-1	2.132	2.132	23.5
5	17.92	1	0	-3	4.946	4.951	3.5	33	43.26	1	8	4	2.090	2.093	3.5
6	18.98	1	4	0	4.672	4.671	77.1	34	43.52	2	2	6	2.078	2.080	3.6
7	19.68	2	0	-2	4.507	4.506	34.4	35	43.96	3	8	0	2.058	2.057	4.2

Table 1. Cont.

No.	2 $\theta$ / $^{\circ}$	<i>h</i>	<i>k</i>	<i>l</i>	<i>d</i> <sub>exp</sub> /Å	<i>d</i> <sub>cal</sub> /Å	<i>I</i> / <i>I</i> <sub>0</sub>	No.	2 $\theta$ / $^{\circ}$	<i>h</i>	<i>k</i>	<i>l</i>	<i>d</i> <sub>exp</sub> /Å	<i>d</i> <sub>cal</sub> /Å	<i>I</i> / <i>I</i> <sub>0</sub>
8	19.98	2	2	−1	4.440	4.451	61.4	36	44.62	4	6	−1	2.029	2.028	6.7
9	21.54	0	5	1	4.122	4.109	25.1	37	44.90	1	9	−4	2.017	2.017	3.6
10	21.88	1	3	−3	4.059	4.062	68.8	38	45.36	2	6	5	1.998	1.997	9.0
11	22.22	2	3	0	3.997	4.008	44.1	39	46.44	4	5	2	1.954	1.957	9.9
12	22.74	1	5	0	3.907	3.903	13.6	40	47.16	0	1	8	1.926	1.926	14.8
13	22.98	0	0	4	3.867	3.868	6.8	41	48.16	3	6	−6	1.888	1.888	3.2
14	24.44	1	3	3	3.639	3.641	42.4	42	49.58	3	8	3	1.837	1.837	3.5
15	25.72	0	6	−1	3.461	3.462	58.0	43	50.40	3	9	5	1.809	1.809	7.7
16	26.32	1	3	−4	3.383	3.383	24.4	44	51.54	4	8	−3	1.772	1.772	3.2
17	27.24	0	5	3	3.271	3.285	3.7	45	52.60	2	7	6	1.739	1.740	9.9
18	27.74	2	5	−1	3.213	3.216	6.2	46	53.46	0	1	9	1.713	1.714	4.9
19	28.54	1	0	−5	3.125	3.121	4.6	47	55.40	5	7	−1	1.657	1.656	5.2
20	29.44	3	1	1	3.032	3.026	11.2	48	55.88	3	9	4	1.644	1.644	5.3
21	30.38	3	2	1	2.940	2.938	48.5	49	56.84	4	1	6	1.618	1.619	3.1
22	30.82	1	7	0	2.899	2.905	22.2	50	57.46	2	7	7	1.603	1.602	7.1
23	32.34	3	3	−3	2.766	2.767	14.1	51	59.22	1	9	7	1.559	1.560	3.5
24	32.86	1	6	3	2.723	2.723	11.4	52	61.82	2	3	9	1.500	1.499	3.6
25	34.18	0	7	−3	2.621	2.622	29.9	53	62.16	5	7	−6	1.492	1.492	3.4
26	34.70	2	5	3	2.583	2.583	13.5	54	63.96	6	2	3	1.454	1.455	6.3
27	35.92	0	5	5	2.498	2.504	5.3	55	67.04	7	2	−3	1.395	1.395	3.3
28	38.26	1	4	−6	2.350	2.348	25.0	56	72.60	5	4	7	1.301	1.300	3.1

### 3.3. IR Spectroscopy Analysis

The FTIR spectra of the ligand and the complex  $[\text{Zn}_2(\text{btca})(\text{H}_2\text{O})_4]$  are shown in Figures 3 and 4. Compared with the infrared spectrum of the ligand, the number of infrared absorption bands of the complex is less, and this indicates that the symmetry of the complex is very good. In Figure 4, there is a wide and strong band near  $3390\text{ cm}^{-1}$ , which is assigned to the O–H bonds stretching vibration [17]. Compared with the ligand  $\text{H}_4\text{btca}$ , the O–H stretching vibration absorption peak of the complex is wider, and the deformation vibration peak of the water molecules appears at  $1624\text{ cm}^{-1}$  and there are absorption peaks near  $930\text{ cm}^{-1}$  and  $760\text{ cm}^{-1}$ , which is an evidence for the existence of coordination water molecules [18]. The stretching vibration peak of the C–H bonds in the benzene ring is detected at  $3198\text{ cm}^{-1}$ . The absorption peaks at  $1557\text{ cm}^{-1}$  and  $1406\text{ cm}^{-1}$  are assigned to the asymmetric and symmetric stretching vibration in the carboxyl groups, respectively [19,20], and the bending vibration peak of the C=O bonds is located at  $625\text{ cm}^{-1}$ , all of which are a little lower than the frequency of  $\text{H}_4\text{btca}$  ( $1673\text{ cm}^{-1}$ ,  $1416\text{ cm}^{-1}$ , and  $658\text{ cm}^{-1}$ ). Hence, it is illustrated that the carboxyl oxygen atoms in  $\text{H}_4\text{btca}$  coordinate with Zn(II) and then cause a redshift [21]. Additionally, the stretching vibration peak of Zn–O bonds detected at  $517\text{ cm}^{-1}$  is evidence of the coordination between zinc and oxygen atoms [22].

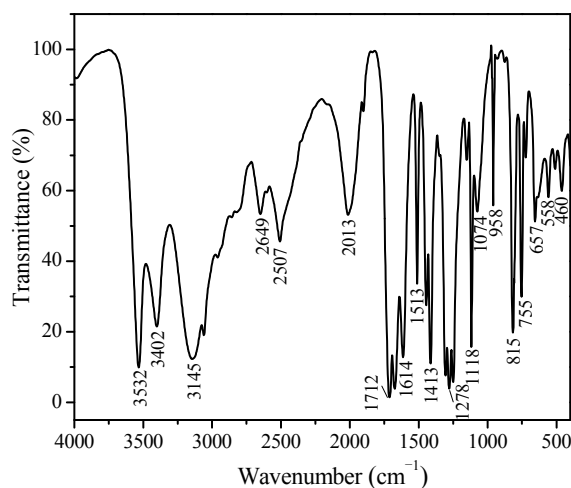


Figure 3. FTIR spectrum of the ligand  $\text{H}_4\text{btca}$ .

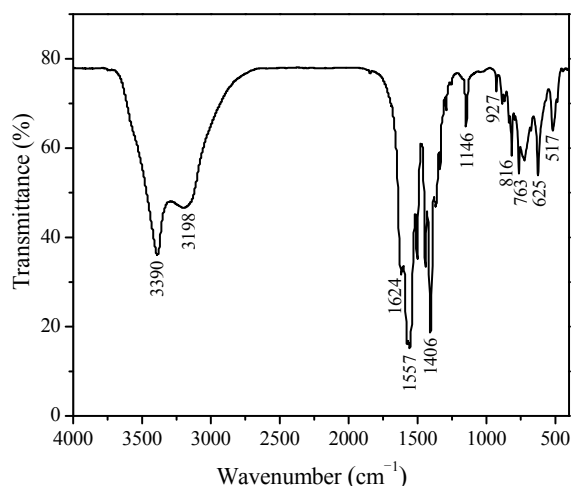


Figure 4. FTIR spectrum of  $[\text{Zn}_2(\text{btca})(\text{H}_2\text{O})_4]$ .

### 3.4. Thermogravimetric Analysis

Studying thermal decomposition of complexes is helpful to understanding of coordination structure and mechanism of thermal decomposition [23]. The thermogravimetric and differential thermogravimetry (TG–DTG) curves of the complex are shown in Figure 5. The TG analysis reveals that the complex is decomposed through two major processes, namely the loss of coordinated water molecules and the oxidative decomposition of the ligand  $\text{btca}^{4-}$  anion. The first weight loss is approximately 15.77% (calcd. 15.91%) near 110 °C, corresponding to loss of four coordination water molecules. The second weight loss occurred at 488 °C is 48.85%, and the final residue is zinc oxide (Found 35.38%, calcd. 35.93%). The decomposition processes can be expressed by the Equation (1) as follows:

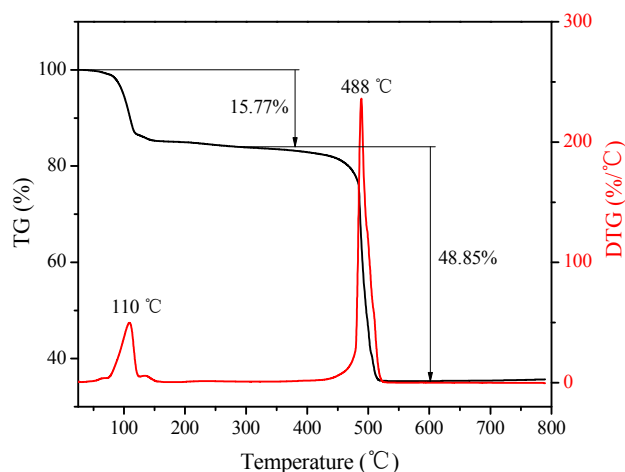
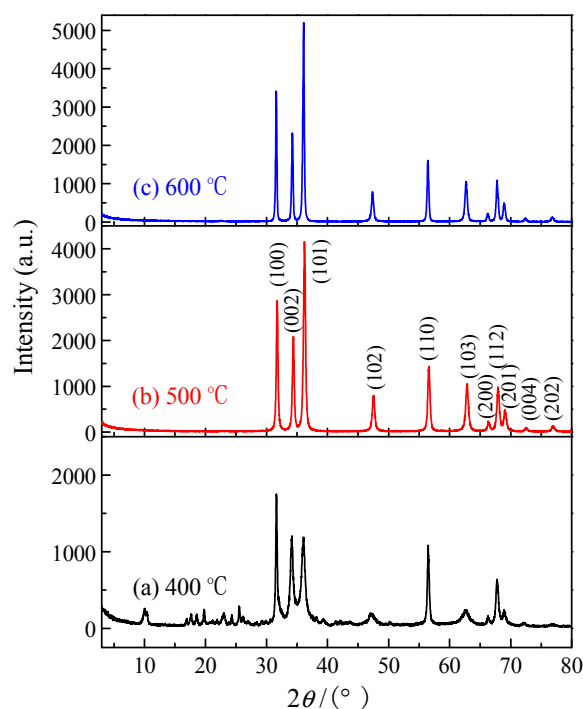


Figure 5. TG–DTG curves of  $[\text{Zn}_2(\text{btca})(\text{H}_2\text{O})_4]$ .

### 3.5. Particle Size and Morphology of Nano-ZnO

In order to expand the application of the title complex, the nanometer zinc oxide was prepared with the complex  $[\text{Zn}_2(\text{btca})(\text{H}_2\text{O})_4]$  as precursor by the thermal decomposition reaction. The complex was respectively calcined at 400 °C, 500 °C, and 600 °C for 1.5 h, and the XRD patterns of the products are shown in Figure 6. At 400 °C, the standard diffraction peaks of the hexagonal system zinc oxide (JCPDS No. 36-1451) is already obtained, while there are some stray peaks, from which we can come

to the conclusion that the complex does not decompose completely. This is also consistent with the thermal decomposition temperature of the complex. In the range of nanometer scale, the smaller the grain size is, the wider and weaker the diffraction peaks will be. As can be seen from Figure 6, the diffraction peaks become sharper when the pyrolysis temperature is increased gradually, and this indicates that the grain size of zinc oxide grows gradually and its crystal shape grows more completely. From the calculation by the X-ray single peak Fourier analysis method [24,25], the particle diameters of the nano-ZnO products (a), (b) and (c) are 19 nm, 26 nm, and 32 nm, respectively.



**Figure 6.** XRD patterns obtained by the calcination of  $[\text{Zn}_2(\text{btca})(\text{H}_2\text{O})_4]$  at different temperatures, (a) 400 °C, (b) 500 °C, and (c) 600 °C.

Figure 7 shows the SEM images of the nano-ZnO obtained from calcining the complex  $[\text{Zn}_2(\text{btca})(\text{H}_2\text{O})_4]$  at 500 °C. It is obvious that the particles are agglomerated together, which is a common phenomenon of nanocrystals. The diameter of the particles is about 25 nm, and it is consistent with the calculated value. The purity of nano-ZnO is high, and the content of zinc oxide determined by EDTA complexometric titration is 99.9%. Therefore, the preparation method of the nano-ZnO has an extensive popularization and application value.

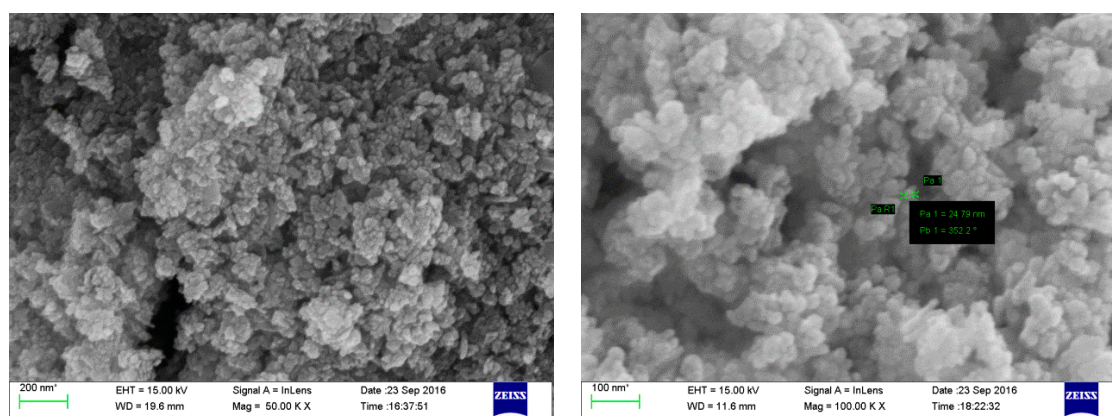


**Figure 7.** SEM images of nano-ZnO.

#### 4. Conclusions

The complex  $[\text{Zn}_2(\text{btca})(\text{H}_2\text{O})_4]$  was synthesized via a solid state reaction at room temperature. The complex was characterized by EA, FTIR, XRD, and TG-DTG. The crystal structure of the complex belonged to monoclinic system with cell parameters  $a = 9.882 \text{ \AA}$ ,  $b = 21.311 \text{ \AA}$ ,  $c = 15.746 \text{ \AA}$ , and  $\beta = 100.69^\circ$ . Every Zn(II) ion was coordinated by four oxygen atoms from two carboxyl groups on the same side of the  $\text{btca}^{4-}$  ligand and two coordinated water molecules. The nano-ZnO was prepared with the complex as a precursor by thermal decomposition. This showed that the grain size of zinc oxide gradually grew with the increase of the pyrolysis temperature. The diameter of the nano-ZnO particles prepared at  $500^\circ\text{C}$  is about 25 nm. The particle size of nano-ZnO can be changed by controlling the pyrolysis temperature of the complex precursor.

**Acknowledgments:** This work was supported by the Longshan academic talent research supporting program of SWUST (No. 17LZX414) and the scientific research funds of Education Department of Sichuan Province (No. 10ZA016).

**Author Contributions:** Mei-Ling Wang and Rong-Gui Yang tied for the first author. Rong-Gui Yang wrote the manuscript. Mei-Ling Wang synthesized the compound and carried on the analysis to EA, FTIR, and TG-DTG. Ting Liu performed the X-ray powder diffraction analysis. Guo-Qing Zhong conceived and designed the experiments. All authors took part in the writing and discussion processes.

**Conflicts of Interest:** The authors declare no conflict of interest.

#### References

1. Xia, C.-K.; Wu, F.; Yang, K.; Wu, Y.-L.; Lu, X.-J. Syntheses, crystal structures and properties of four novel zinc(II) complexes assembled from versatile 1,2,3,5-benzenetetracarboxylic acid and bridging dipyrindyl ligands. *Polyhedron* **2016**, *112*, 78–85. [[CrossRef](#)]
2. Wang, X.-B.; Lu, W.-G.; Zhong, D.-C. Two zinc(II) metal-organic frameworks with mixed ligands of 5-amino-tetrazolate and 1,2,4,5-benzenetetracarboxylate: Synthesis, structural diversity and photoluminescent properties. *J. Solid State Chem.* **2017**, *250*, 83–89. [[CrossRef](#)]
3. Wang, Y.-F.; Li, Z.; Sun, Y.-C.; Zhao, J.-S.; Zhang, S.-C. Synthesis, characterization and crystal structures of 2D Co(II)/Zn(II)-coordination polymers containing 3-(pyridin-4-yl)-5-(pyrazin-2-yl)-1H-1,2,4-triazole and benzenetetracarboxylate co-ligands. *Inorg. Chem. Commun.* **2014**, *44*, 25–28. [[CrossRef](#)]
4. Sanda, S.; Goswami, S.; Jena, H.S.; Parshamoni, S.; Konar, S. A family of three magnetic metal organic frameworks: Their synthesis, structural, magnetic and vapour adsorption study. *CrystEngComm* **2014**, *16*, 4742–4752. [[CrossRef](#)]
5. Zhao, Y.; Lu, H.; Yang, L.; Luo, G.G. Reversible adsorption of a planar cyclic  $(\text{H}_2\text{O})_6$  cluster held in a 2D  $\text{Cu}^{\text{II}}$ -coordination framework. *J. Mol. Struct.* **2016**, *1088*, 155–160. [[CrossRef](#)]
6. Wang, X.-X.; Zhang, M.-X.; Yu, B.; Hecke, K.V.; Cui, G.-H. Synthesis, crystal structures, luminescence and catalytic properties of two  $d^{10}$  metal coordination polymers constructed from mixed ligands. *Spectrochim. Acta A* **2015**, *139*, 442–448. [[CrossRef](#)] [[PubMed](#)]
7. Xia, C.; Yang, K.; Wu, F.; Lu, X.; Min, Y.; Xie, J. Syntheses and characterization of two new compounds based on versatile 1,2,3,5-benzenetetracarboxylic acid and 2,2'-bibenzimidazole. *J. Coord. Chem.* **2017**, *70*, 2510–2519. [[CrossRef](#)]
8. Du, S.; Ji, C.; Xin, X.; Zhuang, M.; Yu, X.; Lu, J.; Lu, Y.; Sun, D. Syntheses, structures and characteristics of four alkaline-earth metal-organic frameworks (MOFs) based on benzene-1,2,4,5-tetracarboxylic acid and its derivative ligand. *J. Mol. Struct.* **2017**, *1130*, 565–572. [[CrossRef](#)]
9. Zhong, G.-Q.; Li, D.; Zhang, Z.-P. Hydrothermal synthesis, crystal structure and magnetic property of a homodinuclear ternary coordination polymer of nickel(II). *Polyhedron* **2016**, *111*, 11–15. [[CrossRef](#)]
10. Wang, G.; Ma, D.; Jia, X.; Cui, X.; Zhao, X.; Wang, Y. In situ preparation of nanometer-scale zinc oxide from zinc acetate in the reaction for the synthesis of dimethyl toluene dicarbamate and its catalytic decomposition performance. *Ind. Eng. Chem. Res.* **2016**, *55*, 8011–8017. [[CrossRef](#)]
11. Lee, T.-H.; Ryu, H.; Lee, W.-J. Fast vertical growth of ZnO nanorods using a modified chemical bath deposition. *J. Alloys Compd.* **2014**, *597*, 85–90. [[CrossRef](#)]

12. Kamari, H.M.; Al-Hada, N.M.; Saion, E.; Shaari, A.H.; Talib, Z.A.; Flaifel, M.H.; Ahmed, A.A.A. Calcined solution-based PVP influence on ZnO semiconductor nanoparticle properties. *Crystals* **2017**, *7*, 2. [[CrossRef](#)]
13. Hussain, S.; Liu, T.; Kashif, M.; Cao, S.; Zeng, W.; Xu, S.; Naseer, K.; Hashim, U. A simple preparation of ZnO nanocones and exposure to formaldehyde. *Mater. Lett.* **2014**, *128*, 35–38. [[CrossRef](#)]
14. Thilagavathi, T.; Geetha, D. Nano ZnO structures synthesized in presence of anionic and cationic surfactant under hydrothermal process. *Appl. Nanosci.* **2014**, *4*, 127–132. [[CrossRef](#)]
15. Zhong, G.-Q.; Zhong, Q. Solid-solid synthesis, characterization, thermal decomposition and antibacterial activities of zinc(II) and nickel(II) complexes of glycine-vanillin Schiff base ligand. *Green Chem. Lett. Rev.* **2014**, *7*, 236–242. [[CrossRef](#)]
16. Li, D.; Zhong, G.-Q.; Wu, Z.-X. Solid-solid synthesis, characterization and thermal decomposition of a homodinuclear cobalt(II) complex. *J. Serb. Chem. Soc.* **2015**, *80*, 1391–1397. [[CrossRef](#)]
17. Tai, X.-S.; Meng, Q.-G.; Liu, L.-L. Synthesis, crystal structure, and cytotoxic activity of a novel eight-coordinated dinuclear Ca(II)-Schiff base complex. *Crystals* **2016**, *6*, 109. [[CrossRef](#)]
18. Nakamoto, K. *Infrared and Raman Spectra of Inorganic and Coordination Compounds*, 6th ed.; John Wiley & Sons Inc.: Hoboken, NJ, USA, 2009.
19. Majumder, A.; Gramlich, V.; Rosair, G.M.; Batten, S.R.; Masuda, J.D.; El Fallah, M.S.; Ribas, J.; Sutter, J.P.; Desplanches, C.; Mitra, S. Five new cobalt(II) and copper(II)-1,2,4,5-benzenetetracarboxylate supramolecular architectures: Syntheses, structures, and magnetic properties. *Cryst. Growth Des.* **2006**, *6*, 2355–2368. [[CrossRef](#)]
20. Lei, R.; Zhang, H.-H.; Hu, J.; Chai, X.-C.; Zhang, S.; Li, C.-X.; Chen, Y.-P.; Sun, Y.-Q. Synthesis and single-crystal structure of a silver(I) carboxyarylphosphonate:  $[\text{Ag}(\text{H}_2\text{BCP})(4,4'\text{-bipy})]\cdot 2\text{H}_2\text{O}$ . *Chin. J. Struct. Chem.* **2010**, *29*, 655–659.
21. Tai, X.S.; You, H.Y. A new 1D chained coordination polymer: Synthesis, crystal structure, antitumor activity and luminescent property. *Crystals* **2015**, *5*, 608–616. [[CrossRef](#)]
22. Bahnasawy, R.M.E.; El-Tabl, A.S.; Shakhdofo, M.M.E.; El-Wahed, N.M.A. Cu(II), Ni(II), Co(II), Mn(II), Zn(II) and Cd(II) complexes of ethyl-3-(2-carbamothioylhydrazono)-2-(hydroxyimino)butanoate: Synthesis, characterization and cytotoxicity activity. *Chin. J. Inorg. Chem.* **2014**, *30*, 1435–1450.
23. Zhong, G.Q.; Shen, J.; Jiang, Q.Y.; Jia, Y.Q.; Chen, M.J.; Zhang, Z.P. Synthesis, characterization and thermal decomposition of  $\text{Sb}^{\text{III}}\text{-M-Sb}^{\text{III}}$  type trinuclear complexes of ethylenediamine-*N,N',N',N'*-tetraacetate (M:Co(II), La(III), Nd(III), Dy(III)). *J. Therm. Anal. Calorim.* **2008**, *92*, 607–616. [[CrossRef](#)]
24. Deacon, G.B.; Phillips, R.J. Relationships between the carbon-oxygen stretching frequencies of carboxylate complexes and the type of carboxylate coordination. *Coord. Chem. Rev.* **1980**, *33*, 227–250. [[CrossRef](#)]
25. Langford, J.I. A rapid method for analysing the breadths of diffraction and spectral lines using the Voigt function. *J. Appl. Cryst.* **1978**, *11*, 10–14. [[CrossRef](#)]

